BNL-211342-2019-JAAM

Thin Film Self-assembly of a Silicon-containing Rod-Coil Liquid Crystalline Block Copolymer

L. Y. Shi, K. Yager

To be published in "Macromolecules"

January 2019

Center for Functional Nanomaterials

Brookhaven National Laboratory

U.S. Department of Energy

USDOE Office of Science (SC), Basic Energy Sciences (BES) (SC-22)

Notice: This manuscript has been authored by employees of Brookhaven Science Associates, LLC under Contract No. DE-SC0012704 with the U.S. Department of Energy. The publisher by accepting the manuscript for publication acknowledges that the United States Government retains a non-exclusive, paid-up, irrevocable, world-wide license to publish or reproduce the published form of this manuscript, or allow others to do so, for United States Government purposes.

DISCLAIMER

This report was prepared as an account of work sponsored by an agency of the United States Government. Neither the United States Government nor any agency thereof, nor any of their employees, nor any of their contractors, subcontractors, or their employees, makes any warranty, express or implied, or assumes any legal liability or responsibility for the accuracy, completeness, or any third party's use or the results of such use of any information, apparatus, product, or process disclosed, or represents that its use would not infringe privately owned rights. Reference herein to any specific commercial product, process, or service by trade name, trademark, manufacturer, or otherwise, does not necessarily constitute or imply its endorsement, recommendation, or favoring by the United States Government or any agency thereof or its contractors or subcontractors. The views and opinions of authors expressed herein do not necessarily state or reflect those of the United States Government or any agency thereof.

Thin Film Self-assembly of a Silicon-containing Rod–Coil Liquid Crystalline Block Copolymer

Ling-Ying Shi,*[†‡] Sangho Lee,[‡] Li-Chen Cheng,[‡] Hejin Huang,[‡] Fen Liao,[†] Rong Ran,[†] Kevin G. Yager,[#] Caroline A. Ross*[‡]

[†]*College of Polymer Science and Engineering, State Key Laboratory of Polymer Materials Engineering, Sichuan University, Chengdu 610065, China*

[‡]*Department of Materials Science and Engineering, Massachusetts Institute of Technology, 77 Massachusetts Avenue, Cambridge, Massachusetts 02139, United States*

[#]*Center for Functional Nanomaterials, Brookhaven National Laboratory, Upton, New York 11973, United States*

* To whom correspondence should be addressed. E-mail: shilingying@scu.edu.cn, caross@mit.edu

KEYWORDS: rod–coil block copolymer; thin film; substrate functionalization; thermal annealing; directed self-assembly

ABSTRACT: The long-range ordering and directed self-assembly of thin films of a high interaction parameter rod–coil liquid crystalline block copolymer (LC BCP),

poly(dimethylsiloxane)-*b*- poly{2,5-bis[(4-methoxyphenyl)-oxycarbonyl]styrene} (PDMS-*b*-PMPCS, or DM), is described. The LC BCP was spin coated on a polystyrene brush-functionalized substrate then thermally annealed at different temperatures with respect to the LC ordering temperature. The effects of the wetting behavior, commensurability between the film thickness and the periodicity, and the LC orientation on the ordering and orientation of the microdomains are described. A monolayer of in-plane cylinders with excellent long-range ordering was produced, and was transferred into SiO_x patterns with tunable sub-10 nm feature sizes. Well-ordered multilayer in-plane cylinders were produced in thicker films, and the structural evolution was studied by GISAXS and GIWAXS. Finally, the cylindrical rod–coil BCP was directed into a novel ladder morphology within lithographically patterned substrate trenches, as well as into patterns of parallel or transverse cylinders. The ordering of cylinders, the ladder morphology, and the etch selectivity and thermal stability of this high-interaction parameter silicon-containing LC rod–coil BCP demonstrate its applicability to nanoscale lithography.

Introduction

The self-assembly of thin films of block copolymers (BCPs) is useful in the formation of periodic nanometer-scale architectures with a wide range of applications including organic optoelectronics, photonic crystals, nanoporous membranes and next-generation nanolithography.[1-6] A high Flory−Huggins interaction parameter χ enables the formation of nanostructures with feature sizes of 10s of nm and below, complementing traditional “top-down” photolithography techniques which are limited by diffraction to feature sizes above ~22 nm.[7,8]

Moreover, high-χ BCPs can exhibit microdomains with small line edge roughness and low defect density.[9,10] There has been considerable study of the thin film behavior of high-χ BCPs consisting of a silicon-containing block such as PDMS (polydimethylsiloxane), PFS (polyferrocenylsilane) and POSS (polyoctahedral silsesquioxanes) combined with an organic block such as polystyrene (PS).[11-16] The high χ ensures a large thermodynamic driving force for microphase separation at relatively low molecular weights.[11-14] Moreover, the silicon-containing BCPs possess natural contrast for facile pattern transfer due to the high etch contrast between the silicon-containing block and the organic component.[11,17,18]

Most work on BCP thin film pattern formation has focused on conventional coil–coil block copolymers,[19,20] but other molecular architectures can provide additional control over the microdomain morphologies.[21,22] Liquid crystalline (LC) rod–coil block copolymers are composed of a block containing LC mesogens and an isotropic block, and can form hierarchically ordered supramolecular structures by interplay between the LC ordering of the mesogens and the microphase separation of the blocks.[23-29] Compared with coil–coil BCPs, a conformationally asymmetrical rod–coil LC BCP can segregate into ordered nanostructures at even lower χN values ($\chi N \geq 5.0$, while $\chi N \geq 10.9$ for coil–coil BCPs),[30] and the phase diagrams are always asymmetrical with stable lamellar phases for large ranges of the volume factions and hexagonal phases observed at very high block fractions, leading to asymmetrical lamellae and thin cylinders.[26,31,32] By tethering a flexible silicon-containing polymer polydimethylsiloxane (PDMS) to an organic rod LC polymer, a class of high-χ LC BCPs can be built which produce hierarchical nanostructures with small feature sizes.[33-35] In previous research, poly(dimethylsiloxane)-*b*-poly{2,5-bis[(4-methoxyphenyl)-oxycarbonyl]styrene} (PDMS-*b*-PMPCS) rod–coil LC block copolymers were synthesized and the bulk phase behavior was

reported, exhibiting a range of nanostructures with feature sizes from 10 to 25 nm.[34] Rod–coil BCPs have been proposed for applications such as photovoltaics.[36,37]

Due to the two competing processes of liquid crystalline ordering and microphase separation in the LC BCPs, one approach to achieve alignment of the microdomains in the thin films is to control the ordering and orientation of the LC mesogens.[38-40] For example, the application of external fields to achieve LC orientation of the side chains can induce macroscopic orientation of the BCP microdomains.[24] For films of rod–coil LC BCPs, anchoring of the LC relative to the substrate can affect the orientation of the lamellar or cylindrical microdomains.[41,42] Apart from experimental investigations of the molecular adsorption of rod–coil BCPs on substrates,[41,43,44] much of the research on thin film self-assembly and directed self-assembly of rod–coil BCPs has been based on simulations[45,46] and experimental investigations of the thin film microdomain ordering and directed self-assembly of rod–coil BCPs remain sparse.

Here, we present an investigation of the thin film morphology and directed self-assembly of an asymmetrical silicon-containing rod–coil block copolymer poly(dimethylsiloxane)-*b*-poly{2,5-bis[(4-methoxyphenyl)-oxycarbonyl]styrene} (PDMS-*b*-PMPCS, or DM) with molecular weight 22 kg/mol and volume fraction of PDMS 25%, in which the PMPCS is a nematic liquid crystalline polymer. In bulk this BCP forms hexagonally packed cylinders within a wide temperature range.[34] Cylindrical microdomains of PDMS in a PMPCS matrix with excellent long-range order have been produced in both thin and thick films by utilizing a PS-brush functionalized silicon substrate and thermal annealing. The PDMS cylindrical microdomains are converted into SiO_x patterns with tunable mesa and trench widths by etching. Moreover, the directed self-assembly of this rod–coil BCP produces an interesting ladder morphology as well as transverse and parallel microdomains within template trenches. This work

illustrates the intriguing possibilities of rod–coil LC BCPs in nanofabrication.

Experimental methods

The substrates consisted of bare silicon wafers with a native oxide layer. Patterned silicon substrates with 100 nm deep trenches of different widths including trench/mesa of 85 nm/ 300 nm and 135 nm/ 90 nm and isolated trenches 135 nm wide were provided by Taiwan Semiconductor Manufacturing Company (TSMC). A polystyrene (PS) brush layer was formed on the surface by first, spin-coating a PS-OH film (~35 nm thickness) from solution (M_n = 11.0 kg/mol, polydispersity index (PDI) = 1.1, Polymer Source, Inc), then baking at 170 °C under vacuum (20 Torr) for 20 h. Upon annealing, the dehydration reaction between hydroxyl groups of the polymer chain and silanol groups of the silicon oxide led to PS chains covalently grafted on the silicon wafer.[47,48] After baking, the substrates were thoroughly rinsed in toluene 5 times to remove excess polymer chains. The thickness of the grafted PS brush layer was measured to be 3 nm by optical ellipsometry.

The PDMS-*b*-PMPCS rod–coil block copolymer was synthesized through atom transfer radical polymerization (ATRP) as reported in previous work.[34] The chemical structure of the PDMS-*b*-PMPCS rod–coil block copolymer is shown in Scheme 1. The polymer used in this study, $D_{4.4k}M_{17.8k}$, had a molar mass of 22.2 kg/mol, in which the molar mass of PDMS and PMPCS were 4.4 and 17.8 kg/mol, respectively and the polydispersity index was 1.07. The volume fraction of the PDMS was f_{PDMS}~0.25. Solutions of the PDMS-*b*-PMPCS were made in toluene with concentration 1.5, 2.5 and 5.0 wt %. Films with thickness ranging from 20 nm to 110 nm were obtained by spin-coating on as-received Si substrates and on the PS brush functionalized silicon substrates at various spin speeds. The film thickness was obtained from a

reflectometry system (FilMetrics F20-UV) by measuring the reflectance spectra of the BCP thin film within a wavelength range of 300 − 1000 nm. The films were thermally annealed at different temperatures under vacuum (20 Torr) for 72 h. Due to the lower surface energy of the PDMS block, a thin wetting layer of PDMS is expected to form at the film/air interface.[49,50]

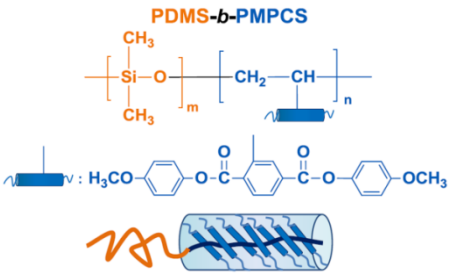

Scheme 1. The chemical structure and structural model of PDMS-*b*-PMPCS rod–coil block copolymer.

The thermally annealed BCP thin films were then subjected to a two-step reactive ion etching (Plasma-Therm 790) consisting of a 50W CF_4 plasma at 15 mTorr for 8 seconds to remove the PDMS wetting layer on the surface and a 90W O_2 plasma at 6 mTorr for 8–30 seconds to selectively etch the PMPCS matrix, leaving oxidized PDMS cylinders on the substrates. The morphologies of the etched BCP thin films were characterized using a Zeiss Merlin high resolution scanning electron microscopy (SEM) at 2 kV. The morphologies of the BCP thin films before and after etch were characterized by atomic force microscopy (AFM) experiments in both height and phase-contrast modes using a Veeco Metrology Nanoscope V scanned probe microscope controller with a Dimension 3100 AFM in tapping mode.

Grazing-incidence small-angle X-ray scattering (GISAXS) and wide-angle X-ray scattering (GIWAXS) measurements were performed at the Complex Materials Scattering (CMS,

11-BM) beamline of the National Synchrotron Light Source II at Brookhaven National Laboratory. A 110 nm thick film was measured by in-situ GISAXS and GIWAXS during a thermal cycling consisting of room temperature–120–140–160–180–200 ^{o}C and held for 5 - 10 min at each temperature. An ex-situ GISAXS measurement was also made on a film that had been annealed at 200 ^{o}C under vacuum (20 Torr) for 72 h.

Results and Discussion

The PDMS-*b*-PMPCS (DM) block copolymer is an example of a high interaction parameter rod–coil liquid crystalline block copolymer which can provide a variety of nanostructures with small feature sizes.[34] The interaction parameter χ of this rod–coil BCP cannot be measured using X-ray scattering because the order–disorder transition temperature is above the decomposition temperature of the BCP. However, it may be estimated from the difference in solubility parameter (δ) between the blocks. Considering the coil–coil high-χ BCP PS-*b*-PDMS, the solubility parameters of PS (δ_{PS}=18.5 $J^{1/2}cm^{3/2}$) and PDMS (δ_{PDMS}=15.0 $J^{1/2}cm^{3/2}$) have a difference of approximately 3.5 $J^{1/2}cm^{3/2}$.[51] In comparison the solubility parameter of PMPCS is calculated to be about 21.8 $J^{1/2}cm^{3/2}$,[34] therefore the δ difference between the PMPCS and PDMS is about twice that between the PS and PDMS, implying a χ value about four times higher. Moreover the PMPCS has a higher monomer volume than PS further increasing χ, given by $\chi=V_0(\delta_{PMPCS}-\delta_{PDMS})^2/kT$ with V_0 the segment volume, yielding an estimate of χ=886/T.

For the PMPCS block, the steric crowding of the bulky mesogenic side chains causes the polymer backbone to become a quasi-linear rod-like chain.[52] In bulk, the $D_{4.4k}M_{17.8k}$ with f_{PDMS} ~

25% and rod length L_{rod} ~10.7 nm self-assembles into a hexagonal (HEX) structure of close-packed PDMS cylinders in a PMPCS matrix after annealing at temperatures from 120 to 160 ^{o}C. The rod-like PMPCS block, which has a glass transition temperature T_g of 109 ^{o}C, undergoes an entropy-driven transition to a nematic liquid crystalline phase above 160 ^{o}C.[34] The LC ordering is improved as the temperature increases (also, when the molecular weight of the PMPCS is lower, a higher temperature is required for the LC to order). In addition, for this LC block copolymer, once the PMPCS rods develop into the nematic LC phase, the LC ordering remains unchanged upon heating up to decomposition or upon cooling to room temperature, i.e. the nematic structure is preserved once formed. The LC BCP partially transforms to a LAM (lamellar) structure when the temperature increases to 180 ^{o}C. The order-disorder transition of this BCP is higher than the decomposition temperature so a disordered structure is not observed on further heating.

We first describe the structural evolution of the films on a bare silicon substrate as a function of the annealing temperature. The film thickness was 33 - 38 nm measured on different substrates, indicating nonuniformity in the wetting behavior. The samples were thermally annealed at 120 ^{o}C (just above T_g of the PMPCS block), at 160 ^{o}C (above T_g and around the LC ordering temperature) and at 200 ^{o}C (where PMPCS has formed the ordered nematic LC phase).

A series of SEM images of the self-assembled structures on silicon after etching as a function of thermal annealing temperature is shown in Figure 1 and Figure S1. The thickness of the as-cast film and 120 ^{o}C-annealed films did not show terracing over large areas (Figures S1(a,b)). Figure S1(d) shows the presence of PDMS spheres and short worm-like structures in the as-cast film indicating microphase separation during the casting process. When the film was annealed at 120 ^{o}C (Figure S1(e)), a disordered interconnected cylindrical morphology was

observed which develops from the as-cast structure just above the glass transition temperature of the rod block. When the annealing temperature increased to 160 ^{o}C, terracing occurred, indicated by the occurrence of macroscopic brighter holes as shown in Figure S1(c) in SI and Figure 1(a). The terrace formation is due to incommensurability between the polymer film thickness and the in-plane microdomain period.[53] As seen in Figure 1(b), the thinner regions show single layer in-plane cylinders with numerous branches and dislocations, whereas the thicker region in Figure 1(c) presents an interconnected bilayer of cylinders. When the annealing temperature is 200 ^{o}C, terracing is also observed, and the cylinders are more highly ordered (Figures 1(d–f)), especially in the double layer regions. The upper layer of PDMS cylinders appears brighter than the lower layer.[54]

Figure 2(a) shows the AFM height image of the thin films after annealing at 160 ^{o}C before plasma etching in which terraces are visible. The profiles in Figure 2(b) record the height variation along the green lines indicated in Figure 2(a), showing that the step heights are ~17.1 nm. The in-plane center-to-center spacing of the cylinders L_{cc} is ~21.5 nm (Figure 1(b,f)) and for a close-packed cylinder array the layer spacing is expected to be $L_{cc}\sqrt{3}/2$, or 18.6 nm, similar to the measured step height in the unetched film.

In Figures 2(c,d) AFM height and phase images of the film annealed at 160 ^{o}C and then etched show comparable cylinder morphology to the SEM images of etched films. For comparison, AFM height and phase images of the unetched film are shown in Figures S2(a,b), corresponding to the etched sample (Figures 2(c,d)) but with lower contrast. The results demonstrate that the plasma etching did not alter the morphology. The AFM images of the thin film after annealing at 200 ^{o}C, Figures 2(e,f), exhibit better order than those of the 160˚C annealed film.

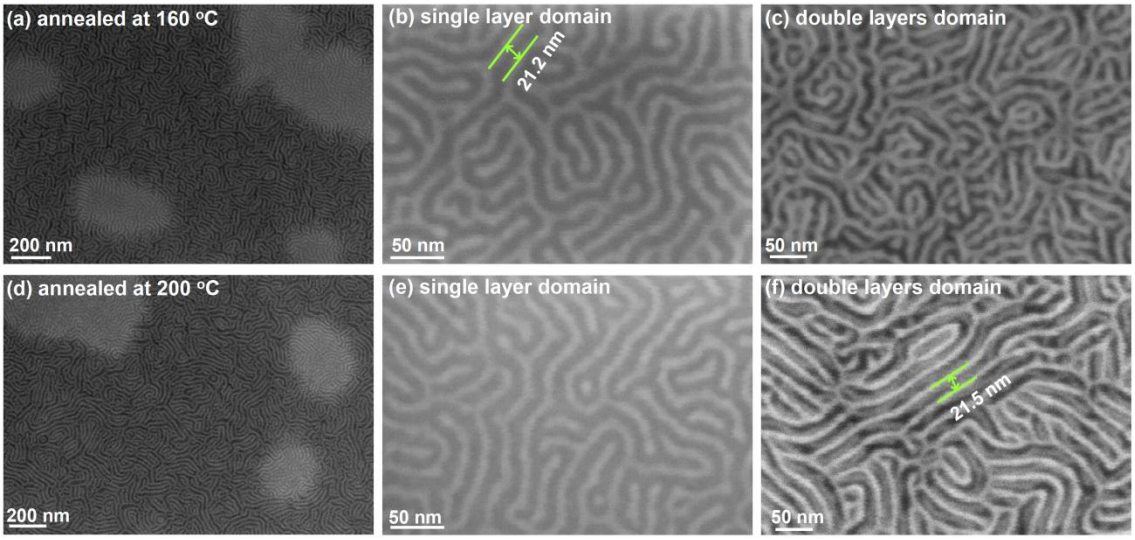

Figure 1. Representative SEM images of oxidized PDMS cylindrical nanopatterns formed in DM rod–coil BCP thin films on bare silicon wafers after annealing at 160 ^{o}C (top, a–c), and 200 ^{o}C (bottom, d–f) and etching. The low magnification images show terracing (a and d), and the high magnification images show single (b and e) and double layer regions (c and f).

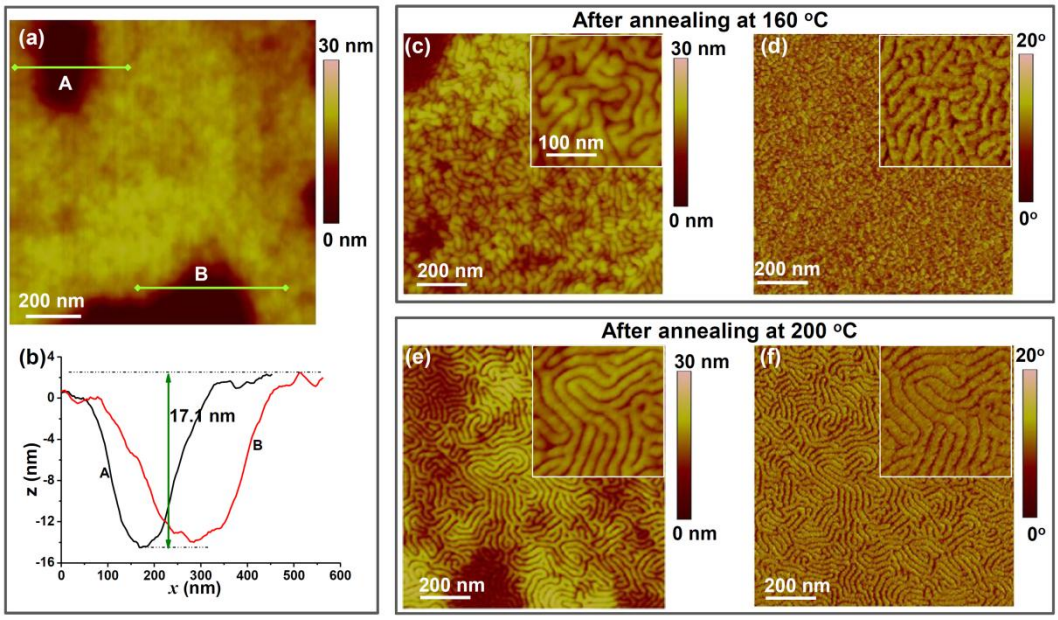

Figure 2. AFM height image (a) of the thin film annealed at 160 ^{o}C before etching with the

profiles (b) tracing the height variation along the green lines indicated in (a). Representative AFM height images (c and e) and phase images (d and f) of the thin films on bare silicon substrates annealed at 160 ^{o}C, and 200 ^{o}C, respectively, then etched, with higher magnification insets.

In-plane microdomain morphologies are expected for this rod–coil BCP thin film due to the dissimilar surface energies between the rod and the coil blocks. The PDMS wets both substrate and air interfaces (symmetrical wetting) and the commensurate film thickness is therefore expected to be an integer number of layer spacings,[48] leading to terrace formation for the film thickness used here. The improved ordering at 200 ^{o}C compared to 160 ˚C annealing is attributed to the LC undergoing nematic ordering and the enhancement of the chain diffusivity of the rod block.

We now discuss the effect of a PS brush, which is preferentially wetted by the majority LC block. Unannealed 33 nm thick films on a PS-brushed substrate exhibit uniform thickness without terracing (Figures S1(f,g)), and poorly organized interconnected PDMS wormlike cylinders representing the kinetically trapped state of the as-spun thin film from the toluene solution. For the 33 nm film annealed at 160 ^{o}C, regions of monolayer and bilayer cylinders were found as shown in Figure S1(h) Figure 3(a). Compared with the morphology observed in the sample on the bare silicon in Fig 1(b), the monolayer cylinders are more uniform with fewer branches and defects. The center-to-center distance of the cylinders is 22.0 nm, similar to that on bare Si. Considering that the length of the LC rods is 10.7 nm, it is likely that the rods interdigitate in the microphase-separated structure. Figure 3(c) shows that the double layer regions also have a better ordered structure than observed in the film on bare silicon and the

upper cylinders lie between the lower ones. AFM confirms the cylindrical morphologies, as shown in Figures 4(a,b).

When the thin films on PS brush modified substrates were annealed at 200 ^{o}C, correlation lengths exceeded several micrometers as shown in Figures 3(d,e) and 4(c,d). As indicated in Figure 3(d), only one defect (junction) occurred within an image area of 1.5 μm × 0.9 μm, and thus the defect density was less than ~0.01 defects/μm^2. A cross-section SEM image of the thin film shows monolayer cylindrical patterns on the substrate as seen in Figure 3(f). The bilayer islands, Figure S3, consisted of parallel cylinders in the two layers. These results show that long-range ordering of this rod–coil BCP is improved by using a PS brush modified substrate and 200 ˚C annealing temperature. An improvement in ordering kinetics by using a brush layer is consistent with observations of coil–coil PS-*b*-PDMS.[47,48,50]

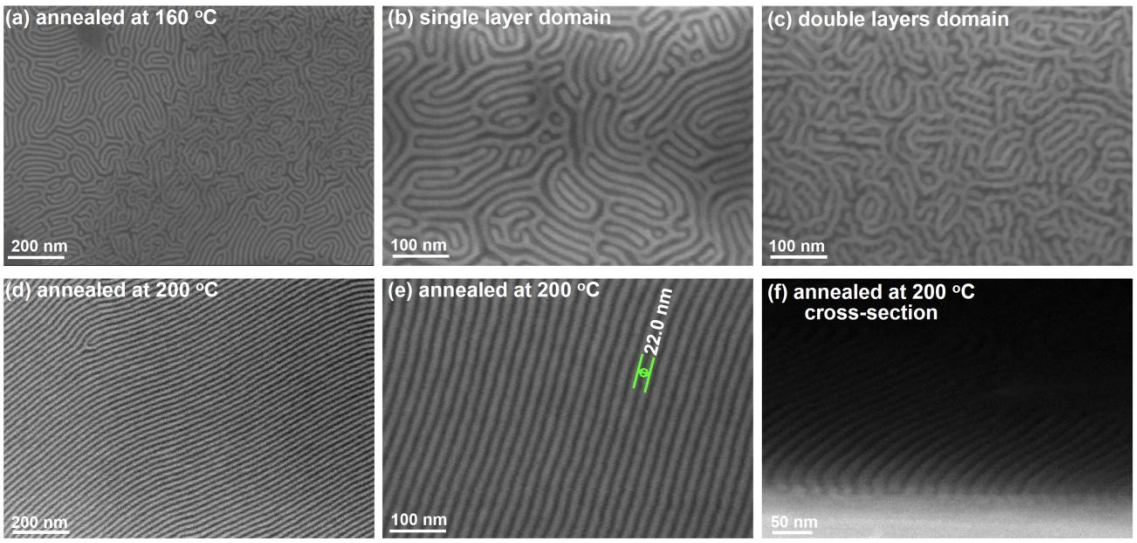

Figure 3. Representative top-view SEM images of PDMS cylindrical structures formed in etched thin films of DM rod–coil BCP on PS-brush modified silicon substrate after annealing at 160 ^{o}C (top, a–c) and 200 ^{o}C (bottom, d–e), and a cross-section SEM image (f) of ordered in-plane

cylinders after annealing at 200 ^{o}C.

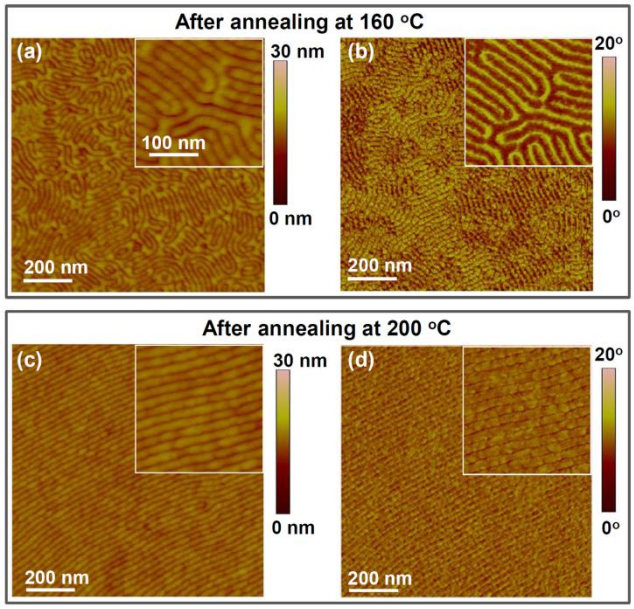

Figure 4. AFM height images (left) and phase images (right) of the thin films on the PS-brush layer modified substrates annealed at 160 ^{o}C (a and b), and 200 ^{o}C (c and d). The insets are higher magnification images.

The dramatic enhancement in ordering of the DM rod–coil block copolymer on the PS-coated substrate at higher temperature may be discussed in terms of the wetting behavior and the LC ordering of the rod blocks. The majority rod block forms a wetting layer on the substrate and the PDMS wets the air interface. This leads to asymmetric wetting where the commensurate film thickness should be[48] $(n+1/2)L_0$ where L_0 is the layer spacing. In our experiment, the film thickness (33 nm) is higher than the commensurate thickness $1.5L_0$ (29 nm) where L_0 = 19 nm is calculated from the center-center distance of the cylinders, L_{cc} = 22 nm. The film is predicted to form a single layer of cylindrical microdomains with bilayer islands, as observed. For the thin film annealed at 160 ^{o}C, the PMPCS rods have not undergone nematic ordering and have the

tendency to be partially adsorbed on the substrate with the long molecular axes parallel to the surface.[43] This produces an incommensurate terraced structure schematically illustrated in Figure 5(a) and the proposed molecular arrangement is illustrated in Figure 5(b). When the annealing temperature increased to 200 ^{o}C, the PMPCS rods on the substrate are expected to be vertically oriented to achieve maximum LC ordering. This contributes to a better ordered commensurate monolayer arrangement as illustrated in Figure 5(c,d). In addition, the nematic LC ordering of the PMPCS provides an additional driving force for microphase separation to achieve a highly ordered nanostructure.

The thin film morphologies remained cylindrical even after annealing at 200 ^{o}C whereas the bulk sample transformed from HEX to a LAM structure above 180 ^{o}C. Moreover, the center to center distance (L_{cc} ~ 22 nm) of the cylinders in the thin films is much smaller than the cylinder to cylinder distance (~28 nm) in the bulk material annealed at 150 ˚C. (This cylinder to cylinder distance was determined from the small angle x-ray scattering data which gave a layer spacing of 25 nm for the bulk material, which corresponds to $L_{cc}\sqrt{3}/2$.) This suggests a different degree of interdigitation between the LC blocks in bulk vs. thin film. The period of the bulk material decreased on annealing at higher temperatures as the LC ordering improved. In bulk the partial transformation to the asymmetrical LAM structure is driven by the LC ordering, but the morphological transition is suppressed in the films, perhaps because of differences in the initial ordering of the LC.

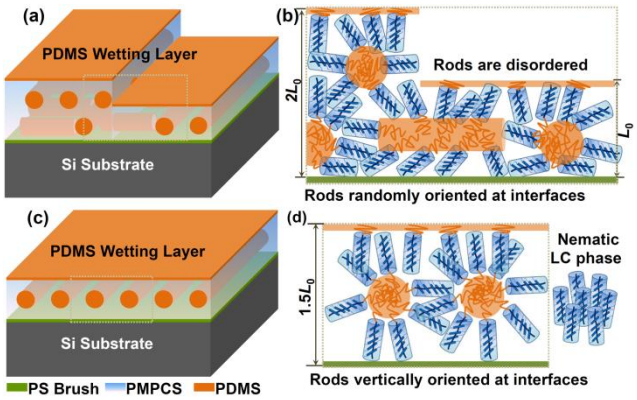

Figure 5. Schematic illustrations of the film morphologies (left) with the molecular arrangements (right) in the indicated cross sections for the thin films on the PS-brush functionalized substrates after annealing at 160 ^{o}C (a and b), and 200 ^{o}C (c and d). At 160 ^{o}C, there is poor nematic ordering and the PMPCS rods are misoriented at the interfaces and at the intermaterial dividing surfaces. At 200 ^{o}C, the nematic ordering of the rod block is improved with the rods preferentially perpendicular to the interfaces and the intermaterial dividing surfaces.

Tunable fine-scale patterns were produced in silica by pattern transfer from the silicon-containing DM rod–coil block copolymer, controlling the feature sizes via the O_2 plasma etching time. The pattern transfer process is schematically illustrated in Figures 6(a–d). The SEM images of the ordered sample after etching in CF_4 then O_2 are shown in Figures 6(e,e′), in which the diameter of the SiO_x cylinders is about 12.5 nm and the space between the cylinders is about 9.5 nm. Based on the cross-section of the etched thin film in Figure 3f, the PDMS wetting layer on the surface and part of the PMPCS between the PDMS cylinders are removed, and the depth of the etched spaces between the cylinders is less than the film thickness. The high χ leads to sharp interfaces and a smooth edge of the transferred pattern. After an additional 10 s etching by the O_2 plasma, the diameter of the cylinders decreased to 9.8 nm and the gap between the cylinders

increased to 12.2 nm (Figures 6(f,f′)), without an observable degradation of edge roughness. The further removal of the PMPCS blocks gives a greater etch depth and higher contrast in the SEM image. After a further 10 s O_2 plasma etch, the cylinder diameter was 7.3 nm and the gap was 14.7 nm (Figures 6(g,g′)). The cylinders remained continuous even at the lowest widths, and the line edge roughness is still lower than 2 nm despite the oxidation of the PDMS. The feature size control with low line edge roughness makes this material attractive for nanofabrication.

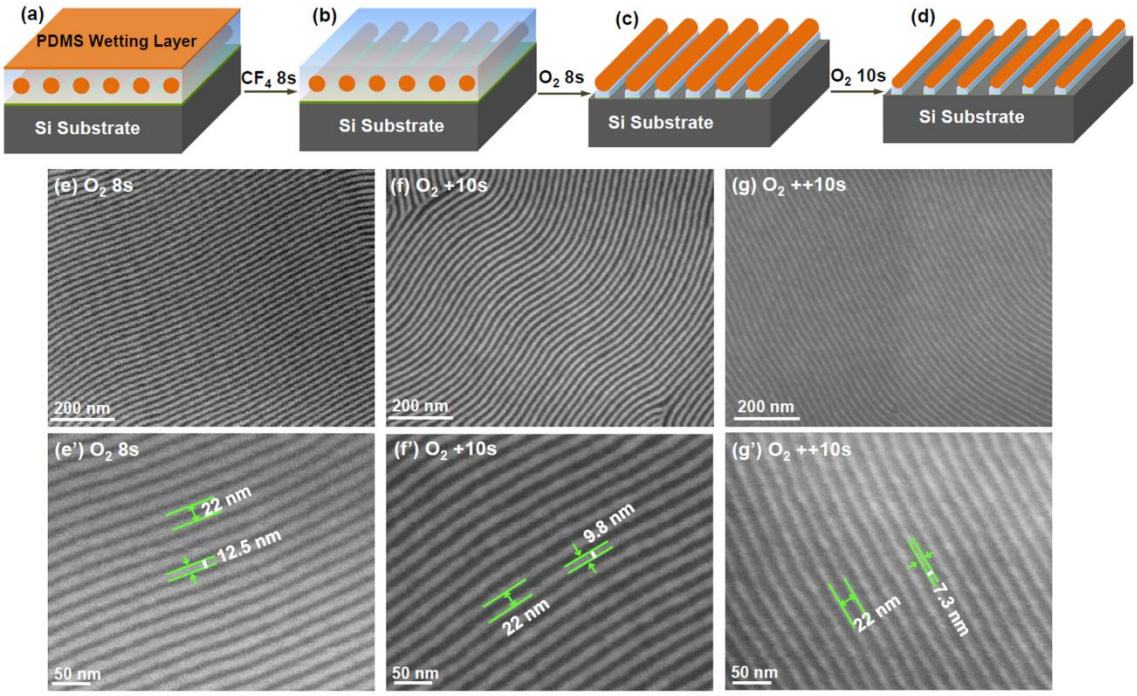

Figure 6. Schematic illustration of the pattern transfer process from the ordered monolayer cylindrical nanostructure: (a) the thin film of ordered monolayer in-plane cylinders of the rod–coil BCP, (b) after removing the PDMS wetting layer by CF_4, (c) the transferred SiO_x pattern with wide cylinders and narrow gaps after a short O_2 plasma etching, and (d) the transferred SiO_x pattern with narrow cylinders and wide gaps after longer O_2 plasma etching. Representative SEM images of transferred SiO_x patterns with etching conditions of CF_4 8 s and

O_2 plasma 8 s (e and e′), with an additional O_2 plasma 10 s noted as +10s (f and f′) and with further additional O_2 plasma 10 s noted as ++10s (g and g′).

To clarify the structural evolution of the BCP during annealing, we examined a 110 nm thick as-cast film on a PS-brush-modified substrate in situ during thermal annealing using GISAXS and GIWAXS. Figures 7(a–c) and Figure S4 present the GISAXS profiles at different temperatures. The as-cast film exhibits very weak scattering (Figure 7a), indicative of a disordered morphology. From 120 to 160 ^{o}C, the block copolymer microphase-separated into cylindrical nanostructures with three-dimensionally random orientation indicated by the distinct rings appearing in the GISAXS images, Figure S4(a,b) and Figure 7b. The poorly ordered interconnected cylindrical morphologies are also confirmed by the SEM results (Figure S5). As the temperature increased to 180 and 200 ^{o}C, the scattering peaks (Figure S4c and Figure 7c)) become more intense and higher order peaks appear, indicative of a well-ordered cylinder morphology with primarily in-plane orientation. The simultaneous GIWAXS experimental results are shown in Figure S6. The scattering ring at q_r = 0.382 Å^{-1} significantly intensified at 180 and 200 ^{o}C, which confirms the improvement of the LC ordering. These results demonstrate an association between the long-range ordering of the microdomains and the LC ordering. Moreover, after thermal annealing for 72 h at 200 ^{o}C, the GISAXS of the 110 nm thick film presents intense Bragg reflections of the hexagonally packed in-plane cylinders, with scattering peaks at q_r = 0.0269 Å^{-1}, corresponding to a *d*-spacing 23.3 nm, Figures 7 (d,e). The grain-size correlation length (ξ) is 442 nm and the full width at half maximum (σ) is as low as 0.0006 Å^{-1}, indicative of a highly ordered nanostructure. The *d*-spacing increased with annealing temperature as shown in Figure 7f, tending to a value of d = 23.3 nm and L_{cc} = 27 nm after a long anneal at

200 °C, which is close to the corresponding values of the bulk sample. The long-rang ordered multilayer in-plane cylindrical morphology after annealing at 200 °C is also confirmed by the SEM image, Figure 7(g), and in-plane fingerprint-like cylindrical patterns are shown in Figure 7(h). The undulations in the cylinders are a result of overetching which reveals the lower layers of cylinders. These results show that through substrate modification and thermal annealing, long-range ordered multilayer cylinders can be produced in thicker films.

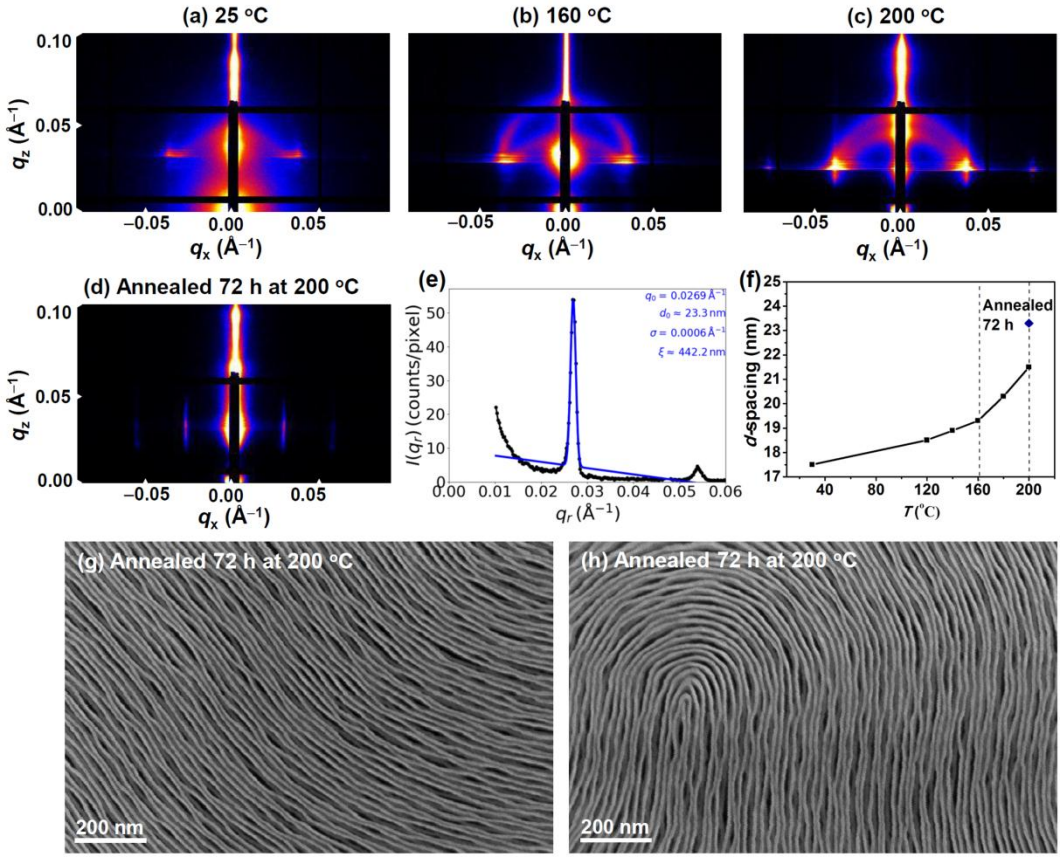

Figure 7. (a–c) Real-time in situ GISAXS 2D patterns of the 110 nm thick as cast film during thermal annealing at 25, 160 and 200 °C (left to right). (d) The GISAXS 2D pattern and (e) the corresponding line cut profile of the thermally annealed thick film at 200 °C for 72 h. (f) The *d*-spacing vs. temperature obtained from the GISAXS line cut results. (g, h) Representative top-

view SEM images of multilayer PDMS cylindrical structures formed in etched 110 nm thick films of DM rod–coil BCP on PS-brush modified silicon substrate after annealing at 200 ^{o}C for 72 h.

We finally demonstrate directed self-assembly of monolayer microdomains of the DM rod-coil BCP within topographical trenches, integrating bottom-up BCP self-assembly with top-down conventional lithography. The 100 nm-deep trench templates with trench width 85 nm and mesa width 300 nm or with trench width 135 nm and mesa width 90 nm as well as 100 nm-deep isolated trenches were obtained by photolithography, and were functionalized with a PS–OH brush layer. Thin films of the rod–coil BCP (1.5~2.5 wt% in toluene) were spin-coated in the same way as described for unpatterned substrates and then annealed at 200 ^{o}C for 72 h. During thermal annealing, the BCP on the 90 nm mesas flowed into the trenches leaving a wetting layer on the mesas, while for wide trenches only the BCP near the mesa edge flowed into the trenches (Figure S7). Based on the initial thickness and the widths of the trenches and the mesas from which the BCP flowed, and assuming a wetting layer of thickness $L_0/2$ is left on the depleted sections of the mesas, the BCP thickness in the trenches was estimated.

For the 85 nm trenches with wide mesas and in the isolated 135 nm wide trenches, the thickness in the trench was about 28 nm, Figure 8 and Figure S7a. Ladder morphologies of the PDMS block were observed in the trenches. Mass transport due to the capillary flow from the mesas into the trenches leads to microdomain orientation parallel to the flow, e.g. cylinders transverse to the trench, but subsequent alignment of cylinders parallel to the sidewalls leads to a reorientation upon further annealing.[13,49] In our experiment, the PS-brush-functionalized sidewalls promotes the formation of a wetting layer of the rod block at the trench wall, and the

PMPCS rods form a nematic LC phase which is oriented perpendicular to the sidewall, indicated by the agreement of the gap distance between the sidewall and the side rails of the ladder (about 13.5 nm, which includes the 3.0 nm PS brush layer) and the length of the rod (10.7 nm). The distance between the centers of neighboring rungs of the ladder is 22.0 nm which matches the periodicity of the cylinders in the film on a flat surface, and the width of the PMPCS domain is about 11.0 nm which agrees with the length of the rods. The transverse orientation of the PDMS rungs enables the equilibrium spacing to be maintained independent of the trench width. The molecular arrangement of the ladder morphology in the trench is schematically illustrated in Figure 8(c).

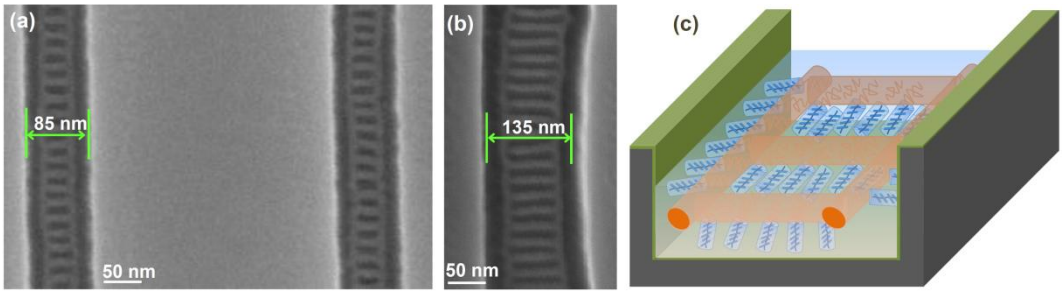

Figure 8. SEM images of ladder morphologies by directed self-assembly of DM rod–coil BCP in 100 nm deep trench templates with (a) trench width of 85 nm and mesa width of 300 nm, and (b) isolated trenches with width of 135 nm. (c) Schematic illustration of the molecular arrangement of the rod–coil BCP in the trench.

The 135 nm trenches with narrow mesas (90 nm) presented morphologies consisting of parallel cylinders, Figures 9 (a,b) with thickness-dependent orientation. When the thickness in the trench was 27 nm (based on an as-spun thickness of 20 nm), the PDMS microdomains aligned transverse to the side wall, with side rails, T junctions or 90º bends observed in some

locations, Figure 9(a). This transverse alignment occurred for a single layer of cylinders in the trench and is similar to the ladder morphology described previously. The stable transverse orientation of the cylinders was also seen for partly-filled trenches as shown in Figure S8(a). Well-ordered transverse cylinders are shown in Figure S9(a).

However, when the thickness of the BCP in the 135 nm-wide trenches was 46 nm (based on as-spun thickness of 31 nm), the LC BCP formed in-plane cylindrical microdomains aligned parallel to the trench walls, Figure 9(b) and Figure S9(b). The bilayer cylinders can be distinguished by the different contrast of the cylinders in the top layer and bottom layer as shown in Figure S10. The well-ordered morphology in the trench corresponds to commensurability both between the layer spacing and film thickness and between cylinder period and trench width. The trench width of 135 nm is commensurate with center-center distance L_{cc} of 22 nm, thus 6 rows of cylinders aligned in the trench. The film thickness in the trench 46 nm is close to 2.5 L_0 (47.5 nm), corresponding to unsymmetrical wetting for a bilayer of cylinders.

A film with estimated thickness of 56 nm in the same topographical substrate, Figure S8(b), shows multilayer cylinders and a transition in the number of cylinders between 7 rows and 6 rows in the trench. The cylinder-cylinder distance near the sidewall is smaller than that at the center of the trench or the unconfined period. A 75 nm thick film in Figure S8(c) presents a disordered interconnected cylindrical structure in the trench. From these results, we can conclude that the morphology in the topographic substrate is influenced by the ratio of the trench width to mesa width, which controls film thickness and capillary flow, and by commensurability in both width and thickness of the polymer in the trench. The confined morphologies of this rod–coil block copolymer in topographical trenches with different dimensions are summarized in Figure 9c.

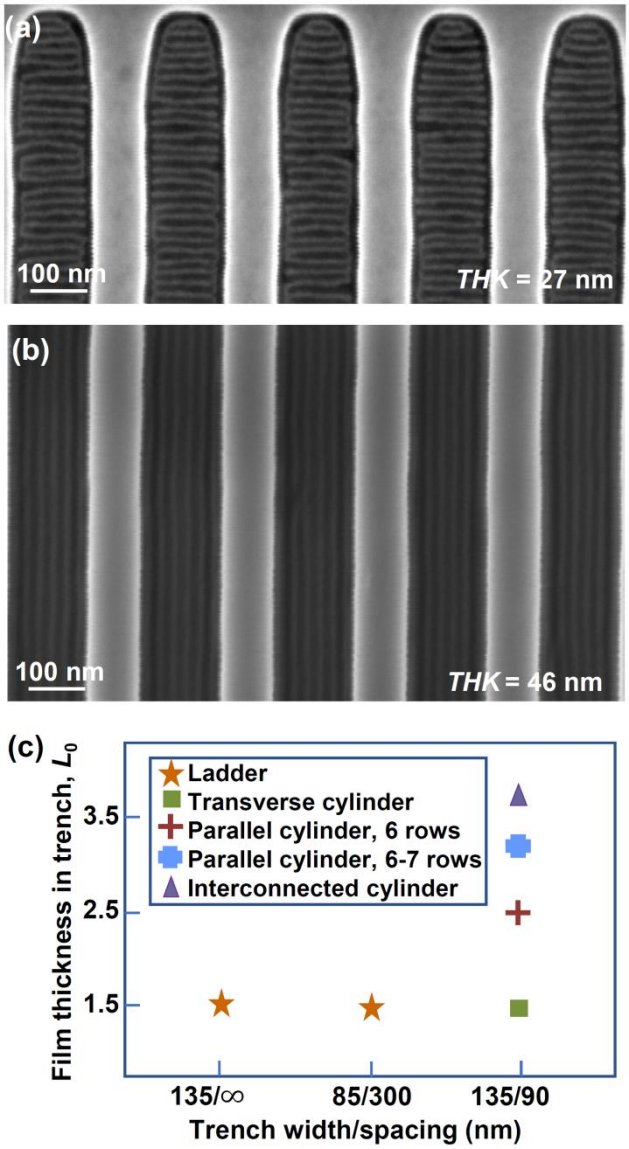

Figure 9. Templated self-assembly in topographic confinements of 100 nm deep trench with trench width of 135 nm and mesa width of 90 nm. (a) SEM images of ordered arrays of oxidized PDMS microdomains transverse to the sidewall in a trench with estimated film thickness 27 nm. (b) SEM images of ordered arrays of oxidized PDMS microdomains aligned parallel to the sidewall in the trench with estimated thickness 46 nm. (c) Summary of the dependence of the template morphologies on the film thickness and the ratio of the trench width to mesa width.

Conclusions

In summary, the self-assembly of films of PDMS-*b*-PMPCS rod–coil LC BCP was investigated on a flat substrate and in topographical trenches. Cylindrical morphologies with different degrees of ordering were observed on flat silicon substrates with symmetrical or unsymmetrical wetting behavior and with the rods in an amorphous state or with LC ordering. In situ scattering measurements show that both LC ordering and microdomain ordering are enhanced at ~180 C. The best ordered monolayer and multilayer in-plane cylindrical microdomains were achieved by using a PS brush functionalized substrate and an annealing temperature of 200 ^{o}C. The monolayer in-plane cylinder patterns were transferred into SiO_x lines with a ~22 nm pitch size, and the ratio of SiO_x line width to gap width changed from 1.3 to 0.5 on increasing the etch time. Ladder-shaped morphologies, transverse cylinders and parallel cylinders were obtained by directed self-assembly in a PS-brush functionalized topographic trench substrate. The long-range ordered morphology on the flat surface and the novel ladder morphology in the grooves are promising for nanopatterning applications, and the presence of the ordered rod block enables additional routes for three-dimensional structure control.

ASSOCIATED CONTENT

Supporting Information.

The following files are available free of charge.

Additional SEM images with different magnifications of oxidized PDMS nanopatterns formed in DM rod–coil BCP thin films on different substrates and after different thermal

annealing; and the AFM height images and phase images of the thin films after annealed at 160 ^{o}C without plasma etching; additional real-time in situ GISAXS 2D patterns; additional SEM images of oxidized PDMS nanopatterns formed in 110 nm thick films; real-time in situ GIWAXS 2D patterns and 1D profiles of a 110 nm thick film during thermal annealing; additional SEM images of the templated self-assembly on different topographical substrates.

AUTHOR INFORMATION

Corresponding Author

* E-mail: shilingying@scu.edu.cn

* E-mail: caross@mit.edu

Author Contributions

The manuscript was written through contributions of all authors. All authors have given approval to the final version of the manuscript.

Notes

The authors declare no competing financial interest.

ACKNOWLEDGMENT

Financial support from NSF DMR-1606911 and the National Natural Science Foundation of China (Grant 51403132) are gratefully acknowledged. Shared experimental facilities of CMSE, an NSF MRSEC under award DMR-1419807, and the NanoStructures Laboratory were used. This research used resources of the Center for Functional Nanomaterials, and the National Synchrotron Light Source II, which are U.S. DOE Office of Science Facilities, at Brookhaven National Laboratory under Contract No. DE-SC0012704.

REFERENCES

(1) Bates, F. S.; Hillmyer, M. A.; Lodge, T. P.; Bates, C. M.; Delaney, K. T.; Fredrickson, G. H. Multiblock Polymers: Panacea or Pandora's Box? *Science* **2012**, *336*, 434.

(2) Russell, T. P.; Chai, Y. 50th Anniversary Perspective: Putting the Squeeze on Polymers: A Perspective on Polymer Thin Films and Interfaces. *Macromolecules* **2017**, *50*, 4597-4609.

(3) Tavakkoli K. G, A.; Nicaise, S. M.; Gadelrab, K. R.; Alexander-Katz, A.; Ross, C. A.; Berggren, K. K. Multilayer block copolymer meshes by orthogonal self-assembly. *Nat. Commun.* **2016**, *7*, 10518.

(4) Suh, H. S.; Kim, D. H.; Moni, P.; Xiong, S.; Ocola, L. E.; Zaluzec, N. J.; Gleason, K. K.; Nealey, P. F. Sub-10-nm patterning via directed self-assembly of block copolymer films with a vapour-phase deposited topcoat. *Nat. Nanotechnol.* **2017**, *12*, 575.

(5) Tang, C.; Wu, W.; Smilgies, D.-M.; Matyjaszewski, K.; Kowalewski, T. Robust Control of Microdomain Orientation in Thin Films of Block Copolymers by Zone Casting. *JACS* **2011**, *133*, 11802-11809.

(6) Ahn, H.; Park, S.; Kim, S.-W.; Yoo, P. J.; Ryu, D. Y.; Russell, T. P. Nanoporous Block Copolymer Membranes for Ultrafiltration: A Simple Approach to Size Tunability. *ACS Nano* **2014**, *8*, 11745-11752.

(7) Sinturel, C.; Bates, F. S.; Hillmyer, M. A. High χ–Low N Block Polymers: How Far Can We Go? *ACS Macro Lett.* **2015**, *4*, 1044-1050.

(8) Bates, C. M.; Bates, F. S. 50th Anniversary Perspective: Block Polymers—Pure Potential. *Macromolecules* **2017**, *50*, 3-22.

(9) Bates, C. M.; Seshimo, T.; Maher, M. J.; Durand, W. J.; Cushen, J. D.; Dean, L. M.; Blachut, G.; Ellison, C. J.; Willson, C. G. Polarity-Switching Top Coats Enable Orientation of Sub–10-nm

Block Copolymer Domains. *Science* **2012**, *338*, 775.

(10) Jeong, J. W.; Park, W. I.; Kim, M.-J.; Ross, C. A.; Jung, Y. S. Highly Tunable Self-Assembled Nanostructures from a Poly(2-vinylpyridine-b-dimethylsiloxane) Block Copolymer. *Nano Lett.* **2011**, *11*, 4095-4101.

(11) Lo, T.-Y.; Krishnan, M. R.; Lu, K.-Y.; Ho, R.-M. Silicon-containing block copolymers for lithographic applications. *Prog. Polym. Sci.* **2018**, *77*, 19-68.

(12) van Genabeek, B.; de Waal, B. F. M.; Gosens, M. M. J.; Pitet, L. M.; Palmans, A. R. A.; Meijer, E. W. Synthesis and Self-Assembly of Discrete Dimethylsiloxane–Lactic Acid Diblock Co-oligomers: The Dononacontamer and Its Shorter Homologues. *JACS* **2016**, *138*, 4210-4218.

(13) Aissou, K.; Mumtaz, M.; Fleury, G.; Portale, G.; Navarro, C.; Cloutet, E.; Brochon, C.; Ross, C. A.; Hadziioannou, G. Sub-10 nm Features Obtained from Directed Self-Assembly of Semicrystalline Polycarbosilane-Based Block Copolymer Thin Films. *Adv. Mater.* **2015**, *27*, 261-265.

(14) Chang, J.-B.; Son, J. G.; Hannon, A. F.; Alexander-Katz, A.; Ross, C. A.; Berggren, K. K. Aligned Sub-10-nm Block Copolymer Patterns Templated by Post Arrays. *ACS Nano* **2012**, *6*, 2071-2077.

(15) Cheng, J. Y.; Mayes, A. M.; Ross, C. A. Nanostructure engineering by templated self-assembly of block copolymers. *Nat. Mater.* **2004**, *3*, 823.

(16) Lee, S.; Cheng, L.-C.; Gadelrab, K. R.; Ntetsikas, K.; Moschovas, D.; Yager, K. G.; Avgeropoulos, A.; Alexander-Katz, A.; Ross, C. A. Double-Layer Morphologies from a Silicon-Containing ABA Triblock Copolymer. *ACS Nano* **2018**, *12*, 6193-6202.

(17) Kun-Hua, T.; Wubin, B.; George, L.; Konstantinos, N.; Apostolos, A.; Caroline, A. R. Universal pattern transfer methods for metal nanostructures by block copolymer lithography.

Nanotechnology **2015**, *26*, 375301.

(18) Wu, N. L. Y.; Harris, K. D.; Buriak, J. M. Conversion of Bilayers of PS-b-PDMS Block Copolymer into Closely Packed, Aligned Silica Nanopatterns. *ACS Nano* **2013**, *7*, 5595-5606.

(19) Hamley, I. W. Ordering in thin films of block copolymers: Fundamentals to potential applications. *Prog. Polym. Sci.* **2009**, *34*, 1161-1210.

(20) Ji, S.; Wan, L.; Liu, C.-C.; Nealey, P. F. Directed self-assembly of block copolymers on chemical patterns: A platform for nanofabrication. *Prog. Polym. Sci.* **2016**, *54-55*, 76-127.

(21) Cheng, L.-C.; Gadelrab, K. R.; Kawamoto, K.; Yager, K. G.; Johnson, J. A.; Alexander-Katz, A.; Ross, C. A. Templated Self-Assembly of a PS-Branch-PDMS Bottlebrush Copolymer. *Nano Lett.* **2018**, *18*, 4360-4369.

(22) Huang, M.; Yue, K.; Huang, J.; Liu, C.; Zhou, Z.; Wang, J.; Wu, K.; Shan, W.; Shi, A.-C.; Cheng, S. Z. D. Highly Asymmetric Phase Behaviors of Polyhedral Oligomeric Silsesquioxane-Based Multiheaded Giant Surfactants. *ACS Nano* **2018**, *12*, 1868-1877.

(23) Olsen, B. D.; Segalman, R. A. Self-assembly of rod–coil block copolymers. *Mater. Sci. Eng. R Rep.* **2008**, *62*, 37-66.

(24) Yu, H. Photoresponsive liquid crystalline block copolymers: From photonics to nanotechnology. *Prog. Polym. Sci.* **2014**, *39*, 781-815.

(25) Olsen, B. D.; Shah, M.; Ganesan, V.; Segalman, R. A. Universalization of the Phase Diagram for a Model Rod−Coil Diblock Copolymer. *Macromolecules* **2008**, *41*, 6809-6817.

(26) Tang, J.; Jiang, Y.; Zhang, X.; Yan, D.; Chen, J. Z. Y. Phase Diagram of Rod–Coil Diblock Copolymer Melts. *Macromolecules* **2015**, *48*, 9060-9070.

(27) Olsen, B. D.; Gu, X.; Hexemer, A.; Gann, E.; Segalman, R. A. Liquid Crystalline Orientation of Rod Blocks within Lamellar Nanostructures from Rod−Coil Diblock Copolymers.

Macromolecules **2010**, *43*, 6531-6534.

(28) Osuji, C.; Ferreira, P. J.; Mao, G.; Ober, C. K.; Vander Sande, J. B.; Thomas, E. L. Alignment of Self-Assembled Hierarchical Microstructure in Liquid Crystalline Diblock Copolymers Using High Magnetic Fields. *Macromolecules* **2004**, *37*, 9903-9908.

(29) Muthukumar, M.; Ober, C. K.; Thomas, E. L. Competing Interactions and Levels of Ordering in Self-Organizing Polymeric Materials. *Science* **1997**, *277*, 1225-1232.

(30) Lee, M.; Cho, B.-K.; Zin, W.-C. Supramolecular Structures from Rod−Coil Block Copolymers. *Chem. Rev.* **2001**, *101*, 3869-3892.

(31) Matsen, M. W.; Schick, M. Microphases of a Diblock Copolymer with Conformational Asymmetry. *Macromolecules* **1994**, *27*, 4014-4015.

(32) Olsen, B. D.; Segalman, R. A. Nonlamellar Phases in Asymmetric Rod−Coil Block Copolymers at Increased Segregation Strengths. *Macromolecules* **2007**, *40*, 6922-6929.

(33) Nickmans, K.; Murphy, J. N.; de Waal, B.; Leclère, P.; Doise, J.; Gronheid, R.; Broer, D. J.; Schenning, A. P. H. J. Sub-5 nm Patterning by Directed Self-Assembly of Oligo(Dimethylsiloxane) Liquid Crystal Thin Films. *Adv. Mater.* **2016**, *28*, 10068-10072.

(34) Shi, L.-Y.; Zhou, Y.; Fan, X.-H.; Shen, Z. Remarkably Rich Variety of Nanostructures and Order–Order Transitions in a Rod–Coil Diblock Copolymer. *Macromolecules* **2013**, *46*, 5308-5316.

(35) Nickmans, K.; Bögels Gerardus, M.; Sánchez‐Somolinos, C.; Murphy Jeffrey, N.; Leclère, P.; Voets Ilja, K.; Schenning Albertus, P. H. J. 3D Orientational Control in Self‐Assembled Thin Films with Sub‐5 nm Features by Light. *Small* **2017**, *13*, 1701043.

(36) Yuan, K.; Chen, L.; Chen, Y. Photovoltaic performance enhancement of P3HT/PCBM solar cells driven by incorporation of conjugated liquid crystalline rod-coil block copolymers. *J. Mater.*

Chem. C **2014**, *2*, 3835-3845.

(37) Guo, C.; Lin, Y.-H.; Witman, M. D.; Smith, K. A.; Wang, C.; Hexemer, A.; Strzalka, J.; Gomez, E. D.; Verduzco, R. Conjugated Block Copolymer Photovoltaics with near 3% Efficiency through Microphase Separation. *Nano Lett.* **2013**, *13*, 2957-2963.

(38) Fukuhara, K.; Nagano, S.; Hara, M.; Seki, T. Free-surface molecular command systems for photoalignment of liquid crystalline materials. *Nat. Commun.* **2014**, *5*, 3320.

(39) Morikawa, Y.; Nagano, S.; Watanabe, K.; Kamata, K.; Iyoda, T.; Seki, T. Optical Alignment and Patterning of Nanoscale Microdomains in a Block Copolymer Thin Film. *Adv. Mater.* **2006**, *18*, 883-886.

(40) Wang, T.; Li, X.; Dong, Z.; Huang, S.; Yu, H. Vertical Orientation of Nanocylinders in Liquid-Crystalline Block Copolymers Directed by Light. *ACS Appl. Mater. Interfaces* **2017**, *9*, 24864-24872.

(41) Park, J.-W.; Cho, Y.-H. Surface-Induced Morphologies in Thin Films of a Rod−Coil Diblock Copolymer. *Langmuir* **2006**, *22*, 10898-10903.

(42) Kim, J.-H.; Rahman, M. S.; Lee, J.-S.; Park, J.-W. Self-Organization of an Amphiphilic Rod−Coil−Rod Block Copolymer into Liquid Crystalline, Substrate-Supported Monolayers and Bilayers. *Macromolecules* **2008**, *41*, 3181-3189.

(43) Kim, J.-H.; Rahman, M. S.; Lee, J.-S.; Park, J.-W. Liquid Crystalline Ordering in the Self-Assembled Monolayers of Tethered Rodlike Polymers. *JACS* **2007**, *129*, 7756-7757.

(44) Jeong, S.-M.; Song, M.; Park, J.-W. Adsorption/desorption-induced phase transformation in the self-assembled monolayers of an amphiphilic rod-coil block copolymer. *Soft Matter* **2012**, *8*, 1309-1312.

(45) Su, Y.-J.; Ma, Z.-X.; Huang, J.-H. Assembly structure and rod orientation of rod–coil

diblock copolymer films. *Polym. J.* **2016**, *48*, 875.

(46) Yang, G.; Tang, P.; Yang, Y.; Wang, Q. Self-Assembled Microstructures of Confined Rod−Coil Diblock Copolymers by Self-Consistent Field Theory. *J. Phys. Chem. B* **2010**, *114*, 14897-14906.

(47) Borah, D.; Rasappa, S.; Senthamaraikannan, R.; Kosmala, B.; Shaw, M. T.; Holmes, J. D.; Morris, M. A. Orientation and Alignment Control of Microphase-Separated PS-b-PDMS Substrate Patterns via Polymer Brush Chemistry. *ACS Appl. Mater. Interfaces* **2013**, *5*, 88-97.

(48) Gu, W.; Hong, S. W.; Russell, T. P. Orienting Block Copolymer Microdomains with Block Copolymer Brushes. *ACS Nano* **2012**, *6*, 10250-10257.

(49) Li-Chen, C.; Wubin, B.; Eduardo Fernandez, M.; Kun-Hua, T.; Konstantinos, N.; George, L.; Apostolos, A.; Ross, C. A. Morphology, directed self-assembly and pattern transfer from a high molecular weight polystyrene-block-poly(dimethylsiloxane) block copolymer film. *Nanotechnology* **2017**, *28*, 145301.

(50) Jung, Y. S.; Ross, C. A. Orientation-Controlled Self-Assembled Nanolithography Using a Polystyrene−Polydimethylsiloxane Block Copolymer. *Nano Lett.* **2007**, *7*, 2046-2050.

(51) Barton, A. F. M. In *Handbook of Polymer-Liquid Interaction Parameters and Solubility Parameters*; CRC Press: Florida, 1990; pp 125-147.

(52) Chen, X.-F.; Shen, Z.; Wan, X.-H.; Fan, X.-H.; Chen, E.-Q.; Ma, Y.; Zhou, Q.-F. Mesogen-jacketed liquid crystalline polymers. *Chem. Soc. Rev.* **2010**, *39*, 3072-3101.

(53) Bai, W.; Hannon, A. F.; Gotrik, K. W.; Choi, H. K.; Aissou, K.; Liontos, G.; Ntetsikas, K.; Alexander-Katz, A.; Avgeropoulos, A.; Ross, C. A. Thin Film Morphologies of Bulk-Gyroid Polystyrene-block-polydimethylsiloxane under Solvent Vapor Annealing. *Macromolecules* **2014**, *47*, 6000-6008.

(54) Tavakkoli K. G, A.; Gotrik, K. W.; Hannon, A. F.; Alexander-Katz, A.; Ross, C. A.; Berggren, K. K. Templating Three-Dimensional Self-Assembled Structures in Bilayer Block Copolymer Films. *Science* **2012**, *336*, 1294.

For Table of Contents Use Only:

Thin Film Self-assembly of a Silicon-containing Rod–Coil Liquid Crystalline Block Copolymer

Ling-Ying Shi,*[†‡] Sangho Lee,[‡] Li-Chen Cheng,[‡] Hejin Huang,[‡] Fen Liao,[†] Rong Ran,[†] Kevin G. Yager,[#] Caroline A. Ross[*,‡]

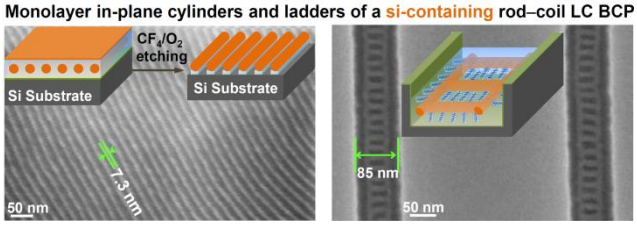

Long-range ordered in-plane cylinders of a silicon-containing rod–coil BCP are produced on functionalized substrates and transferred to SiO_x patterns with sub-10 nm pitch size, and templated self-assembly produces a ladder morphology.